

A kinetic theory approach to model pedestrian dynamics in bounded domains with obstacles

Daewa Kim* and Annalisa Quaini*

*Department of Mathematics, University of Houston, 3551 Cullen Blvd, Houston TX 77204
daewakim@math.uh.edu; quaini@math.uh.edu

June 17, 2019

Abstract We consider a kinetic theory approach to model the evacuation of a crowd from bounded domains. The interactions of a person with other pedestrians and the environment, which includes walls, exits, and obstacles, are modeled by using tools of game theory and are transferred to the crowd dynamics. The model allows to weight between two competing behaviors: the search for less congested areas and the tendency to follow the stream unconsciously in a panic situation. For the numerical approximation of the solution to our model, we apply an operator splitting scheme which breaks the problem into two pure advection problems and a problem involving the interactions. We compare our numerical results against the data reported in a recent empirical study on evacuation from a room with two exits. For medium and medium-to-large groups of people we achieve good agreement between the computed average people density and flow rate and the respective measured quantities. Through a series of numerical tests we also show that our approach is capable of handling evacuation from a room with one or more exits with variable size, with and without obstacles, and can reproduce lane formation in bidirectional flow in a corridor.

1 Introduction

The complex dynamical behavior of pedestrian crowds has fascinated researchers from various scientific fields since the early 1950's. Academic studies started with empirical observations and continued with the development of models in the field of applied physics and mathematics. The simulation of pedestrian flow has attracted increasing research attention in recent years since a reliable simulation model for pedestrian flow may greatly benefit engineers in mass transportation management, and designers in urban planning and architecture.

A very large variety of models have been developed over the years. The different mathematical models can be divided into three main categories depending on the scale of observation [8]. A first approach corresponds to the macroscopic description: evolution equations are derived for mass

density and linear momentum, which are regarded as macroscopic observables of pedestrian flow. See, e.g., [28, 37]. Such an approach is suitable for high density, large-scale systems, which are not the focus of our work.

A second approach looks at the problem at the microscopic level. Microscopic models can be further divided into models which are grid-based or grid-free. Cellular Automata [14, 15, 16, 21, 31] models belong to the first category. They describe pedestrian flow in space-time by assigning discrete states to a grid of space-cells. These cells can be occupied by a pedestrian or be empty. Thus, the movement of pedestrians in space is done by passing them from cell to cell (discrete space) in discrete time. Grid-free methods can be based on second order models (forces-based), first order models (vision-based or speed-based) or zeroth order models (rule-based or decision-based). Force-based models use Newtonian mechanics to interpret pedestrian movement as the physical interaction between the people and the environment, i.e. the action of other people and the environment on a given pedestrian is modeled with forces. These models are one of the most popular modeling paradigms of continuous models because they describe the movement of pedestrians qualitatively well. See, e.g., [18, 24, 26, 27, 32, 33, 39, 43] and references therein. Collective phenomena, like unidirectional or bidirectional flow in a corridor, lane formation, oscillations at bottlenecks, the faster-is-slower effect, and emergency evacuation from buildings, are well reproduced. Agent-based models allow for flexibility, extensibility, and capability to realize heterogeneity in crowd dynamics. For examples of vision-based, speed-based, rule-based, and decision-based models we refer to [2, 3, 4, 17, 19, 20] and references therein. Both force-based and agent-based models may introduce artifacts due to the force representation of human behavior, leading to unrealistic backward movement or oscillating trajectories. These artifacts can be reduced by incorporating extra rules and/or elaborate calibrations, at the price of an increased computational cost.

The scale of observation for the third approach is between the previous two. Introduced in [5] and further developed in [1, 6, 7, 9, 10, 11, 12], this approach derives a Boltzmann-type evolution equation for the statistical distribution function of the position and velocity of the pedestrians, in a framework close to that of the kinetic theory of gases. See also [13] for a literature review on this approach. The model proposed in [5, 6, 12] is valid in unbounded domains and with a homogeneous distribution of walking ability for the pedestrians, while the extension to bounded domains is presented in [1] and further explored in [9, 10, 11]. In [9], more general features of behavioral-social dynamics are taken into account. In [10], Monte Carlo simulations are introduced to study pedestrians behavior in complex scenarios. The methodology in [10] is validated by comparing the computed fundamental density-velocity diagrams with empirically observed ones and by checking that well known emerging properties are reproduced. A kinetic theory approach for modeling pedestrian dynamics in presence of social phenomena, such as the propagation of stress conditions, is presented in [11]. Finally, we refer to [7] for a thorough description of how kinetic theory and evolutionary game theory can be used to understand the dynamics of living systems.

The scale of observation for the third approach is between the previous two. In a framework close to that of the kinetic theory of gases, this approach derives a Boltzmann-type evolution equation for the statistical distribution function of the position and velocity of the pedestrians. The kinetic

theory approach was introduced in [5] and further developed in [12]. The model in [5, 12] is valid in unbounded domains. The extension to bounded domains is presented in [1]. Further literature review on this approach can be found in [13].

In this work, we consider the model proposed in [1]. We first validate it against experimental data and then extend it to bounded domains with obstacles. It is worth noticing that most of the models and methods in the references cited so far have been shown to reproduce phenomena of pedestrian movement qualitatively through analysis and/or numerical simulations. However, before using a model to predict quantitative results like, e.g., the total evacuation time, the mathematical models have to be validated and the numerical methods have to be verified [22]. In the context of pedestrian dynamics, this is still difficult due to a lack of reliable experimental data. In addition, the few available datasets show large differences [34, 36, 42]. In this paper, we compare our numerical results against the data reported in a recent empirical study [40]. We have selected this study because it deals with egressing from a facility and thus it is the most directly related to our focus. With the model under consideration, for medium and medium-to-large groups of people we manage to achieve good agreement between the computed average people density and flow rate and the respective measured quantities. Finally, we mention that in order to make the models more reliable, evolutionary adjustment of the parameters and data assimilations have also been proposed in [29, 41], respectively.

The strategy we propose to handle obstacles within the computational domain makes use of an effective obstacle area, which is an enlarged area that encloses the real obstacle, and a model parameter used to describe the quality of the environment. Thanks to those two ingredients, we can successfully exclude from the walkable area square and rectangular obstacles. We test our strategy in a square room that contains one or two obstacles and has one exit. In addition, through a series of numerical tests we show that our approach is capable of handling evacuation from a room with one or more exits with variable size, with and without obstacles, and can reproduce lane formation in bidirectional flow in a corridor.

The paper is organized as follows. Section 2 introduces the representation of the system and the modeling of interactions with pedestrians and with the environment. In Section 3, we apply the Lie splitting algorithm to the model described in Section 2. Numerical results are presented in Section 4 and conclusions are drawn in Section 5.

2 Mathematical model

The model we consider is based on the model proposed in [1]. Let $\Omega \subset \mathbb{R}^2$ denote a bounded domain. We assume that the boundary $\partial\Omega$ includes an exit E which could be the finite union of disjoint sets, and walls W . Here, $\overline{E} \cup \overline{W} = \overline{\partial\Omega}$ and $E \cap W = \emptyset$. Let $\mathbf{x} = (x, y) \in \Omega$ denote position and $\mathbf{v} = v(\cos \theta, \sin \theta) \in \Omega_{\mathbf{v}}$ denote velocity, where v is the velocity modulus, θ is the velocity direction, and $\Omega_{\mathbf{v}} \subset \mathbb{R}^2$ is the velocity domain. For a system composed by a large number

of pedestrians distributed inside Ω , the distribution function is given by

$$f = f(t, \mathbf{x}, \mathbf{v}) \quad \text{for all } t \geq 0, \mathbf{x} \in \Omega, \mathbf{v} \in \Omega_{\mathbf{v}}.$$

Under suitable integrability conditions, $f(t, \mathbf{x}, \mathbf{v})d\mathbf{x}d\mathbf{v}$ represents the number of individuals who, at time t , are located in the infinitesimal rectangle $[x, x + dx] \times [y, y + dy]$ and have a velocity belonging to $[v, v + dv] \times [\theta, \theta + d\theta]$. Since we use polar coordinates for the velocity, we can write the distribution function as $f = f(t, \mathbf{x}, v, \theta)$.

Following [1], we assume that variable θ is discrete. This assumption is motivated by the granularity of pedestrian dynamics when the crowd size is not enough to justify the continuity of the distribution function over the variable θ . For simplicity, we assume θ can take values in the set:

$$I_{\theta} = \left\{ \theta_i = \frac{i-1}{N_d} 2\pi : i = 1, \dots, N_d \right\},$$

where N_d is the maxim number of possible directions. As for the velocity magnitude v , we model it as a continuous deterministic variable which evolves in time and space according to macroscopic effects determined by the overall dynamics. In fact, experimental studies show that in practical situations the speed of pedestrians depends mainly on the level of congestion around them.

Due to the deterministic nature of the variable v , the kinetic type representation is given by the reduced distribution function

$$f(t, \mathbf{x}, \theta) = \sum_{i=1}^{N_d} f^i(t, \mathbf{x}) \delta(\theta - \theta_i), \quad (1)$$

where $f^i(t, \mathbf{x}) = f(t, \mathbf{x}, \theta_i)$ represents the active particles that, at time t and position \mathbf{x} , move with direction θ_i . In equation (1), δ denotes the Dirac delta function.

Let us introduce some reference quantities that will be use to make the variable dimensionless. We define:

- D : the largest distance a pedestrian can cover in domain Ω ;
- V_M : the highest velocity modulus a pedestrian can reach in low density and optimal environmental conditions;
- T : a reference time given by D/V_M ;
- ρ_M : the maximal admissible number of pedestrians per unit area.

The dimensionless variables are then: position $\hat{\mathbf{x}} = \mathbf{x}/D$, time $\hat{t} = t/T$, velocity modulus $\hat{v} = v/V_M$ and distribution function $\hat{f} = f/\rho_M$. From now on, all the variables will be dimensionless and hats will be omitted to simplify notation.

Due to the normalization of f , and of each f^i , the dimensionless local density is obtained by summing the distribution functions over the set of directions:

$$\rho(t, \mathbf{x}) = \sum_{i=1}^{N_d} f^i(t, \mathbf{x}). \quad (2)$$

As mentioned above, we assume that pedestrians adjust their speed depending on the level of congestion around them. This means that the velocity modulus depends formally on the local density, i.e. $v = v[\rho](t, \mathbf{x})$, where square brackets are used to denote that v depends on ρ in a functional way. For instance, v can depend on ρ and on its gradient.

A parameter $\alpha \in [0, 1]$ is introduced to represent the quality of the domain where pedestrians move: $\alpha = 0$ corresponds to the worst quality which forces pedestrians to slow down or stop, while $\alpha = 1$ corresponds to the best quality, which allows pedestrians to walk at the desired speed. We assume that the maximum dimensionless speed v_M a pedestrian can reach depends linearly on the quality of the environment. For simplicity, we take $v_M = \alpha$. Let ρ_c be a critical density value such that for $\rho < \rho_c$ we have free flow regime (i.e., low density condition), while for $\rho > \rho_c$ we have a slowdown zone (i.e., high density condition). We set $\rho_c = \alpha/5$. Note that this choice is compatible with the experimentally measured values of ρ_c reported in [35]. Next, we set the velocity magnitude v equal to v_M in the free flow regime and equal to a heuristic third-order polynomial in the slowdown zone:

$$v = v(\rho) = \begin{cases} \alpha & \text{for } \rho \leq \rho_c(\alpha) = \alpha/5 \\ a_3\rho^3 + a_2\rho^2 + a_1\rho + a_0 & \text{for } \rho > \rho_c(\alpha) = \alpha/5, \end{cases} \quad (3)$$

where a_i is constant for $i = 0, 1, 2, 3$. To set the value of these constants, we impose the following conditions: $v(\rho_c) = v_M$, $\partial_\rho v(\rho_c) = 0$, $v(1) = 0$ and $\partial_\rho v(1) = 0$. This leads to:

$$\begin{cases} a_0 &= (1/(\alpha^3 - 15\alpha^2 + 75\alpha - 125))(75\alpha^2 - 125\alpha) \\ a_1 &= (1/(\alpha^3 - 15\alpha^2 + 75\alpha - 125))(-150\alpha^2) \\ a_2 &= (1/(\alpha^3 - 15\alpha^2 + 75\alpha - 125))(75\alpha^2 + 375\alpha) \\ a_3 &= (1/(\alpha^3 - 15\alpha^2 + 75\alpha - 125))(-250\alpha). \end{cases} \quad (4)$$

Figure 1 (A) reports v as a function of ρ for $\alpha = 0.4, 0.7, 1$.

2.1 Modeling interactions

Each pedestrian is modeled as a particle. Interactions involve three types of particles:

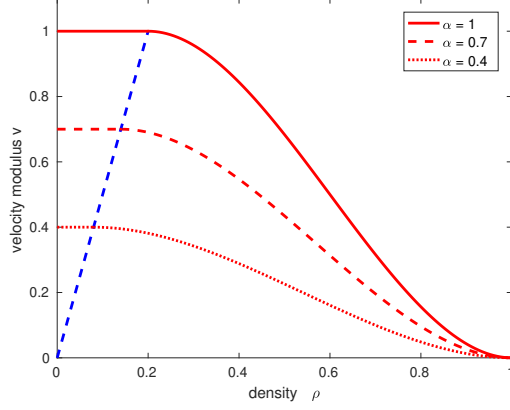
- *test particles* with state (\mathbf{x}, θ_i) : they are representative of the whole system;
- *candidate particles* with state (\mathbf{x}, θ_h) : they can reach in probability the state of the test particles after individual-based interactions with the environment or with field particles;
- *field particles* with state (\mathbf{x}, θ_k) : their presence triggers the interactions of the candidate particles.

The process through which a pedestrian decides the direction to take is the results of several factors. We take into account four factors:

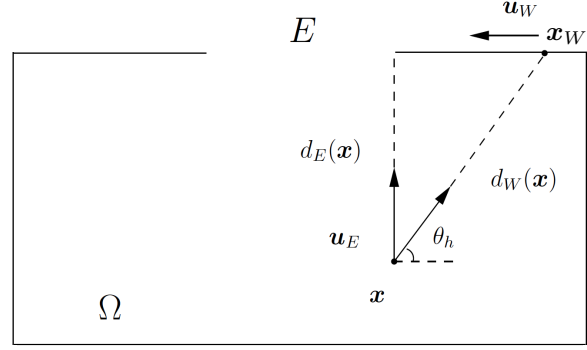
(F1) *The goal to reach the exit.*

Given a candidate particle at the point \mathbf{x} , we define its distance to the exit as

$$d_E(\mathbf{x}) = \min_{\mathbf{x}_E \in E} \|\mathbf{x} - \mathbf{x}_E\|,$$



(a) v as a function of ρ



(b) Notation in a sample computational domain

Figure 1: (A) Dependence of the dimensionless velocity modulus v on the dimensionless density ρ for different values of the parameter α , which represents the quality of the environment. (B) Sketch of computational domain Ω with exit E and a pedestrian located at \mathbf{x} , moving with direction θ_h . The pedestrian should choose direction \mathbf{u}_E to reach the exit, while direction \mathbf{u}_W is to avoid collision with the wall. The distances from the exit and from the wall are d_E and d_W , respectively.

and we consider the unit vector $\mathbf{u}_E(\mathbf{x})$, pointing from \mathbf{x} to the exit. See Figure 1 (B).

(F2) *The desire to avoid the collision with walls.*

Given a candidate particle at the point \mathbf{x} moving with direction θ_h , we define the distance $d_W(\mathbf{x}, \theta_h)$ from the particle to a wall at a point $\mathbf{x}_W(\mathbf{x}, \theta_h)$ where the particle is expected to collide with the wall. The unit tangent vector $\mathbf{u}_W(\mathbf{x}, \theta_h)$ to $\partial\Omega$ at \mathbf{x}_W points to the direction of the the exit. Vector \mathbf{u}_W is used to avoid a collision with the walls. See Figure 1 (B).

(F3) *The tendency to look for less congested area.*

A candidate particle (\mathbf{x}, θ_h) may decide to change direction in order to avoid congested areas. This is achieved with the direction that gives the minimal directional derivative of the density at the point \mathbf{x} . We denote such direction by unit vector $\mathbf{u}_C(\theta_h, \rho)$.

(F4) *The tendency to follow the stream.*

A candidate particle modifies its state, in probability, into that of the test particle due to interactions with field particles, while the test particle loses its state as a result of these interactions. A candidate particle h interacting with a field particle k may decide to follow it and thus adopt its direction, denoted with unit vector $\mathbf{u}_F = (\cos \theta_k, \sin \theta_k)$.

Factors (F1) and (F2) are related to geometric aspects of the domain, while factors (F3) and (F4) consider that people's behavior is strongly affected by surrounding crowd. Note that the effects related to factors (F3) and (F4) compete with each other: (F4) is dominant in a panic situation,

while (F3) characterizes rational behavior. As a weight between (F3) and (F4), we introduce parameter $\varepsilon \in [0, 1]$: $\varepsilon = 0$ corresponds to the situation in which only the research of less congested areas is considered (rational behavior), while $\varepsilon = 1$ corresponds to the situation in which only the tendency to follow the stream is taken into account (panic behavior).

2.1.1 Interaction with the bounding walls

The interaction with the bounding walls is modeled with two terms:

- $\mu[\rho]$: the *interaction rate* models the frequency of interactions between candidate particles and the boundary of the domain. If the local density is getting lower, it is easier for pedestrians to see the walls and doors. Thus, we set $\mu[\rho] = 1 - \rho$.
- $\mathcal{A}_h(i)$: the *transition probability* gives the probability that a candidate particle h , i.e. with direction θ_h , adjusts its direction into that of the test particle θ_i due to the presence of the walls and/or an exit. The following constraint for $\mathcal{A}_h(i)$ has to be satisfied:

$$\sum_{i=1}^{N_d} \mathcal{A}_h(i) = 1 \quad \text{for all } h \in \{1, \dots, N_d\}.$$

We assume that particles change direction, in probability, only to an adjacent clockwise or counterclockwise direction in the discrete set I_θ . This means a candidate particle h may end up into the states $h - 1, h + 1$ or remain in the state h . In the case $h = 1$, we set $\theta_{h-1} = \theta_{N_d}$ and, in the case $h = N_d$, we set $\theta_{h+1} = \theta_1$. The set of all transition probabilities $\mathcal{A} = \{\mathcal{A}_h(i)\}_{h,i=1,\dots,N_d}$ forms the so-called *table of games* that models the game played by active particles interacting with the bounding walls.

To take into account factors (F1) and (F2), we define the vector

$$\begin{aligned} \mathbf{u}_G(\mathbf{x}, \theta_h) &= \frac{(1 - d_E(\mathbf{x}))\mathbf{u}_E(\mathbf{x}) + (1 - d_W(\mathbf{x}, \theta_h))\mathbf{u}_W(\mathbf{x}, \theta_h)}{\|(1 - d_E(\mathbf{x}))\mathbf{u}_E(\mathbf{x}) + (1 - d_W(\mathbf{x}, \theta_h))\mathbf{u}_W(\mathbf{x}, \theta_h)\|} \\ &= (\cos \theta_G, \sin \theta_G). \end{aligned} \tag{5}$$

Here θ_G is the *geometrical preferred direction*, which is the ideal direction that a pedestrian should take in order to reach the exit and avoid the walls in an optimal way. Notice that the closer a pedestrian is to an exit (resp., a wall), the more direction \mathbf{u}_E (resp., \mathbf{u}_W) weights.

A candidate particle h will update its direction by choosing the angle closest to θ_G among the three allowed angles θ_{h-1}, θ_h and θ_{h+1} . The transition probability is given by:

$$\mathcal{A}_h(i) = \beta_h(\alpha)\delta_{s,i} + (1 - \beta_h(\alpha))\delta_{h,i}, \quad i = h - 1, h, h + 1, \tag{6}$$

where

$$s = \arg \min_{j \in \{h-1, h+1\}} \{d(\theta_G, \theta_j)\},$$

with

$$d(\theta_p, \theta_q) = \begin{cases} |\theta_p - \theta_q| & \text{if } |\theta_p - \theta_q| \leq \pi, \\ 2\pi - |\theta_p - \theta_q| & \text{if } |\theta_p - \theta_q| > \pi. \end{cases} \quad (7)$$

In (6), δ denotes the Kronecker delta function. Coefficient β_h , proportional to parameter α , is defined by:

$$\beta_h(\alpha) = \begin{cases} \alpha & \text{if } d(\theta_h, \theta_G) \geq \Delta\theta, \\ \alpha \frac{d(\theta_h, \theta_G)}{\Delta\theta} & \text{if } d(\theta_h, \theta_G) < \Delta\theta, \end{cases}$$

where $\Delta\theta = 2\pi/N_d$. The role of β_h is to allow for a transition to θ_{h-1} or θ_{h+1} even in the case that the geometrical preferred direction θ_G is closer to θ_h . Such a transition is more likely to occur the more distant θ_h and θ_G are. Notice that if $\theta_G = \theta_h$, then $\beta_h = 0$ and $\mathcal{A}_h(h) = 1$, meaning that a pedestrian keeps the same direction (in the absence of interactions other than with the environment) with probability 1.

2.1.2 Interaction with obstacles

The strategy reported in the previous section to avoid collisions with the walls works well when the pedestrian is sufficiently far from the walls. If pedestrians get too close to the bounding walls, and in particular if they are close to an exit, the definition of \mathbf{u}_G in (5) does not prevent collisions with the walls. Thus, obstacles within the domain Ω cannot be avoided just by adjusting \mathbf{u}_W . In this section, we report an effective strategy to handle obstacles.

Four ingredients are needed to exclude the real obstacle area from the walkable domain:

1. An effective area: an enlarged area that encloses the real obstacle.
2. A definition of \mathbf{u}_W to account for the effective area.
3. A setting of the parameter α in the effective area depending on the shape of the obstacle.
4. A dynamic setting of \mathbf{u}_E .

The efficacy of this approach is demonstrated numerically in Sec. 4.3. Given the complexity of the pedestrian dynamics model under consideration, a formal demonstration that this approach guarantees exclusion of the obstacle from the walkable area is less straightforward and we shall address it elsewhere. We note that all the ingredients are already available within the model.

The effective area is necessary especially if the obstacle is close to an exit: it allows to define \mathbf{u}_W with respect to a larger area than the one occupied by the obstacle to achieve the goal of having no pedestrian walking on the real obstacle area. See Fig. 2. In the numerical results reported in Section 4.3, we used an effective area that is four times bigger than the real obstacle area. The size and shape of the effective area has been determined heuristically.

Since some pedestrians will walk on part of the effective area, one needs to set parameter α . By setting $\alpha = 1$ (i.e., best quality of the environment) in the effective area, pedestrians can move with the maximal velocity modulus as they approach the obstacle and thus they quickly adapt to the effective area through \mathbf{u}_W . However, some pedestrians will walk close to the top, bottom, and rear

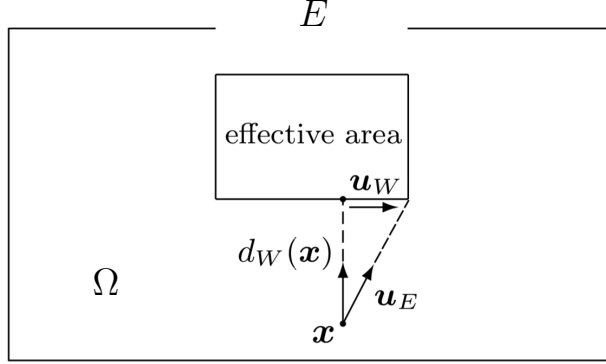


Figure 2: Definition of \mathbf{u}_W and \mathbf{u}_E with respect to the effective area.

(with respect to the pedestrian motion) boundary of the effective area. Thus, the real obstacle is located at the front of the effective area. From the numerical results reported in Section 4.3, we also see that the shape of the obstacle is square. By setting $\alpha = 0$ (i.e., worst quality of the environment) in the effective area, pedestrians are forced to slow down at the front part of the effective area. The slow down leads to higher densities in the front part of the effective area, therefore direction \mathbf{u}_W competes with direction \mathbf{u}_C . As a result some pedestrians walk on the front part of the effective area. However, as the congestion decreases pedestrians avoid the rear part of the effective area. From the numerical results shown in Section 4.3, we see that the shape of the obstacle for $\alpha = 0$ in the effective area is slender.

Finally, the dynamic setting of \mathbf{u}_E is needed for certain pedestrians, depending on their position with respect to the obstacle. As a pedestrian approaches the effective area of an obstacle, \mathbf{u}_E connects his/her position to the closest corner of the effective area in the direction of the final target (i.e., the exit). See Fig. 2. Notice that \mathbf{u}_E can be regarded as the direction a pedestrian needs to take to reach his/her target. Thus, it is reasonable that a pedestrian adjusts the direction when in proximity of an obstacle.

2.1.3 Interactions between pedestrians

The interaction with other pedestrians is modeled with two terms:

- $\eta[\rho]$: the *interaction rate* defines the number of binary encounters per unit time. If the local density increases, then the interaction rate also increases. For simplicity, we take $\eta[\rho] = \rho$. Notice that unlike the case of classical gas dynamics, this rate is not related to the relative particle velocity.
- $\mathcal{B}_{hk}(i)[\rho]$: the *transition probability* gives the probability that a candidate particle h modifies its direction θ_h into that of the test particle i , i.e. θ_i , due to the research of less congested areas and the interaction with a field particle k that moves with direction θ_k . The following

constrain for $\mathcal{B}_{hk}(i)$ has to be satisfied:

$$\sum_{i=1}^{N_d} \mathcal{B}_{hk}(i)[\rho] = 1 \quad \text{for all } h, k \in \{1, \dots, N_d\},$$

where again the square brackets denote the dependence on the density ρ .

The game consists in choosing the less congested direction among the three admissible ones. This direction can be computed for a candidate pedestrian h situated at \mathbf{x} , by taking

$$C = \arg \min_{j \in \{h-1, h, h+1\}} \{\partial_j \rho(t, \mathbf{x})\},$$

where $\partial_j \rho$ denotes the directional derivative of ρ in the direction given by angle θ_j . We have $\mathbf{u}_C(\theta_h, \rho) = (\cos \theta_C, \sin \theta_C)$. As for the tendency to follow the crowd, we set $\mathbf{u}_F = (\cos \theta_k, \sin \theta_k)$. This means that a candidate particle follows the direction of a field particle.

To take into account (F3) and (F4), we define the vector

$$\mathbf{u}_P(\theta_h, \theta_k, \rho) = \frac{\varepsilon \mathbf{u}_F + (1 - \varepsilon) \mathbf{u}_C(\theta_h, \rho)}{\|\varepsilon \mathbf{u}_F + (1 - \varepsilon) \mathbf{u}_C(\theta_h, \rho)\|} = (\cos \theta_P, \sin \theta_P),$$

where the subscript P stands for *pedestrians*. Direction θ_P is the *interaction-based preferred direction*, obtained as a weighted combination between the tendency to follow the stream and the tendency to avoid crowded zones.

The transition probability is given by:

$$\mathcal{B}_{hk}(i)[\rho] = \beta_{hk}(\alpha) \rho \delta_{r,i} + (1 - \beta_{hk}(\alpha) \rho) \delta_{h,i}, \quad i = h-1, h, h+1,$$

where r and β_{hk} are defined by:

$$r = \arg \min_{j \in \{h-1, h, h+1\}} \{d(\theta_P, \theta_j)\},$$

$$\beta_{hk}(\alpha) = \begin{cases} \alpha & \text{if } d(\theta_h, \theta_P) \geq \Delta\theta \\ \alpha \frac{d(\theta_h, \theta_P)}{\Delta\theta} & \text{if } d(\theta_h, \theta_P) < \Delta\theta. \end{cases}$$

We recall that $d(\cdot, \cdot)$ is defined in (7).

2.2 Equation of balance

The derivation of the mathematical model can be obtained by a suitable balance of particles in an elementary volume of the space of microscopic states, considering the net flow into such volume

due to transport and interactions [1]. Taking into account factors (F1)-(F4), we obtain:

$$\begin{aligned}
& \frac{\partial f^i}{\partial t} + \nabla \cdot (\mathbf{v}^i[\rho](t, \mathbf{x}) f^i(t, \mathbf{x})) \\
&= \mathcal{J}^i[f](t, \mathbf{x}) \\
&= \mathcal{J}_G^i[f](t, \mathbf{x}) + \mathcal{J}_P^i[f](t, \mathbf{x}) \\
&= \mu[\rho] \left(\sum_{h=1}^n \mathcal{A}_h(i) f^h(t, \mathbf{x}) - f^i(t, \mathbf{x}) \right) \\
&\quad + \eta[\rho] \left(\sum_{h,k=1}^n \mathcal{B}_{hk}(i)[\rho] f^h(t, \mathbf{x}) f^k(t, \mathbf{x}) - f^i(t, \mathbf{x}) \rho(t, \mathbf{x}) \right)
\end{aligned} \tag{8}$$

for $i = 1, 2, \dots, N_d$. Functional $\mathcal{J}^i[f]$ represents the net balance of particles that move with direction θ_i due to interactions. As explained in the previous subsection, we consider both the interaction with the environment and with the surrounding people. Thus, we can write \mathcal{J}^i as $\mathcal{J}^i = \mathcal{J}_G^i + \mathcal{J}_P^i$, where \mathcal{J}_G^i is an interaction between candidate particles and the environment and \mathcal{J}_P^i is an interaction between candidate and field particles.

Equation (8) is completed with equation (2) for the density and equation (3),(4) for the velocity. In the next section, we will discuss a numerical method for the solution of problem (2),(3),(4),(8).

3 Numerical method

The approach we consider is based on a splitting method that decouples the treatment the transport term and the interaction term in equation (8). As usual with splitting methods, the idea is to split the model into a set of subproblems that are easier to solve and for which practical algorithms are readily available. The numerical method is then completed by picking an appropriate numerical scheme for each subproblem. Among the available operator-splitting methods, we chose the Lie splitting scheme because it provides a good compromise between accuracy and robustness, as shown in [23].

3.1 The Lie operator-splitting scheme

Although the Lie splitting scheme is quite well-known, it may be useful to present briefly this scheme before applying it to the solution of problem (2),(3),(4),(8).

Let us consider a first-order system in time:

$$\begin{aligned}
\frac{\partial \phi}{\partial t} + A(\phi) &= 0, \quad \text{in } (0, T), \\
\phi(0) &= \phi_0,
\end{aligned}$$

where A is an operator from a Hilbert space into itself. Operator A is then split, in a non-trivial decomposition, as

$$A = \sum_{i=1}^I A_i.$$

The Lie scheme consists of the following. Let $\Delta t > 0$ be a time discretization step for the time interval $[0, T]$. Denote $t^k = k\Delta t$, with $k = 0, \dots, N_t$ and let ϕ^k be an approximation of $\phi(t^k)$. Set $\phi^0 = \phi_0$. For $n \geq 0$, compute ϕ^{k+1} by solving

$$\frac{\partial \phi_i}{\partial t} + A_i(\phi_i) = 0 \quad \text{in } (t^k, t^{k+1}), \quad (9)$$

$$\phi_i(t^k) = \phi^{k+(i-1)/I}, \quad (10)$$

and then set $\phi^{k+i/I} = \phi_i(t^{k+1})$, for $i = 1, \dots, I$.

This method is first-order accurate in time. More precisely, if (9) is defined on a finite-dimensional space, and if the operators A_i are smooth enough, then $\|\phi(t^k) - \phi^k\| = O(\Delta t)$ [23].

In the next section, we will apply Lie splitting to problem (8). The whole problem will be split into three subproblems:

1. A pure advection problem in the x direction.
2. A pure advection problem in the y direction.
3. A problem involving the interaction with the environment and other pedestrians.

3.2 Lie scheme applied to problem (8)

Let us apply the Lie operator-splitting scheme described in the previous section to problem (8). Given an initial condition $f^{i,0} = f^i(0, \mathbf{x})$, for $i = 1, \dots, N_d$, the algorithm reads: For $k = 0, 1, 2, \dots, N_t - 1$, perform the following steps:

- **Step 1:** Find f^i , for $i = 1, \dots, N_d$, such that

$$\begin{cases} \frac{\partial f^i}{\partial t} + \frac{\partial}{\partial x} ((v[\rho] \cos \theta_i) f^i(t, \mathbf{x})) = 0 & \text{on } (t^k, t^{k+1}), \\ f^i(t^k, \mathbf{x}) = f^{i,k}. \end{cases} \quad (11)$$

Set $f^{i,k+\frac{1}{3}} = f^i(t^{k+1}, \mathbf{x})$.

- **Step 2:** Find f^i , for $i = 1, \dots, N_d$, such that

$$\begin{cases} \frac{\partial f^i}{\partial t} + \frac{\partial}{\partial y} ((v[\rho] \sin \theta_i) f^i(t, \mathbf{x})) = 0 & \text{on } (t^k, t^{k+1}), \\ f^i(t^k, \mathbf{x}) = f^{i,k+\frac{1}{3}}. \end{cases} \quad (12)$$

Set $f^{i,k+\frac{2}{3}} = f^i(t^{k+1}, \mathbf{x})$.

- **Step 3:** Find f_i , for $i = 1, \dots, N_d$, such that

$$\begin{cases} \frac{\partial f^i}{\partial t} = \mathcal{J}^i[f](t, \mathbf{x}) & \text{on } (t^k, t^{k+1}), \\ f^i(t^k, \mathbf{x}) = f^{i,k+\frac{2}{3}}. \end{cases} \quad (13)$$

Set $f^{i,k+1} = f^i(t^{k+1}, \mathbf{x})$.

Notice that once $f^{i,k+1}$ is computed for $i = 1, \dots, N_d$, we use equation (2) to get the density ρ^{k+1} and equation (3),(4) to get the velocity magnitude at time t^{k+1} .

3.3 Space and time discretization

Let us assume for simplicity that the computational domain under consideration is a rectangle $[0, L] \times [0, H]$, for given L and H . We mesh the computational domain by choosing Δx and Δy to partition interval $[0, L]$ and $[0, H]$, respectively. Let $N_x = L/\Delta x$ and $N_y = H/\Delta y$. We define the discrete mesh points $\mathbf{x}_{pq} = (x_p, y_q)$ by

$$\begin{aligned} x_p &= p\Delta x, & p &= 0, 1, \dots, N_x, \\ y_q &= q\Delta y, & q &= 0, 1, \dots, N_y. \end{aligned}$$

It will also be useful to define

$$\begin{aligned} x_{p+1/2} &= x_p + \Delta x/2 = \left(p + \frac{1}{2}\right)\Delta x, \\ y_{q+1/2} &= y_q + \Delta y/2 = \left(q + \frac{1}{2}\right)\Delta y. \end{aligned}$$

In order to simplify notation, let us set $\phi = f^i$, $\theta = \theta_i$, $t_0 = t^k$, $t_f = t^{k+1}$. Let M be a positive integer (≥ 3 , in practice). We associate with M a time discretization step $\tau = (t_f - t_0)/M$ and set $t^m = t_0 + m\tau$. Next, we proceed with the space and time discretization of each subproblem in Section 3.2.

Step 1

Let $\phi_0 = f^{i,k}$. Problem (11) can be rewritten as

$$\begin{cases} \frac{\partial \phi}{\partial t} + \frac{\partial}{\partial x} ((v[\rho] \cos \theta)\phi(t, \mathbf{x})) = 0 & \text{on } (t_0, t_f), \\ \phi(t_0, \mathbf{x}) = \phi_0. \end{cases} \quad (14)$$

The finite difference method we use produces an approximation $\Phi_{p,q}^m \in \mathbb{R}$ of the cell average

$$\Phi_{p,q}^m \approx \frac{1}{\Delta x \Delta y} \int_{y_{q-1/2}}^{y_{q+1/2}} \int_{x_{p-1/2}}^{x_{p+1/2}} \phi(t^m, x, y) dx dy,$$

where $m = 1, \dots, M$, $1 \leq p \leq N_x - 1$ and $1 \leq q \leq N_y - 1$. Given an initial condition ϕ_0 , function ϕ^m will be approximated by Φ^m with

$$\Phi^m \Big|_{[x_{p-1/2}, x_{p+1/2}] \times [y_{q-1/2}, y_{q+1/2}]} = \Phi_{p,q}^m$$

The Lax-Friedrichs method for problem (14) can be written in conservative form as follows:

$$\Phi_{p,q}^{m+1} = \Phi_{p,q}^m - \frac{\tau}{\Delta x} \left(\mathcal{F}(\Phi_{p,q}^m, \Phi_{p+1,q}^m) - \mathcal{F}(\Phi_{p-1,q}^m, \Phi_{p,q}^m) \right)$$

where

$$\mathcal{F}(\Phi_{p,q}^m, \Phi_{p+1,q}^m) = \frac{\Delta x}{2\tau} (\Phi_{p,q}^m - \Phi_{p+1,q}^m) + \frac{1}{2} \left((v[\rho_{p,q}^m] \cos \theta) \Phi_{p,q}^m + (v[\rho_{p+1,q}^m] \cos \theta) \Phi_{p+1,q}^m \right).$$

Step 2

Let $\phi_0 = f^{i,k+\frac{1}{3}}$. Problem (12) can be rewritten as

$$\begin{cases} \frac{\partial \phi}{\partial t} + \frac{\partial}{\partial y} ((v[\rho] \sin \theta) \phi(t, \mathbf{x})) = 0 & \text{on } (t_0, t_f), \\ \phi(t_0, \mathbf{x}) = \phi_0 \end{cases}$$

Similarly to step 1, we use the conservative Lax-Friedrichs scheme:

$$\Phi_{p,q}^{m+1} = \Phi_{p,q}^m - \frac{\tau}{\Delta y} \left(\mathcal{F}(\Phi_{p,q}^m, \Phi_{p,q+1}^m) - \mathcal{F}(\Phi_{p,q-1}^m, \Phi_{p,q}^m) \right)$$

where

$$\mathcal{F}(\Phi_{p,q}^m, \Phi_{p,q+1}^m) = \frac{\Delta y}{2\tau} (\Phi_{p,q}^m - \Phi_{p,q+1}^m) + \frac{1}{2} \left((v[\rho_{p,q}^m] \sin \theta) \Phi_{p,q}^m + (v[\rho_{p,q+1}^m] \sin \theta) \Phi_{p,q+1}^m \right).$$

Step 3

Let $\mathcal{J} = \mathcal{J}^i$ and $\phi_0 = f^{i,k+\frac{2}{3}}$. Problem (13) can be rewritten as

$$\begin{cases} \frac{\partial \phi}{\partial t} = \mathcal{J}[f](t, \mathbf{x}) & \text{on } (t_0, t_f), \\ \phi(t_0, \mathbf{x}) = \phi_0. \end{cases}$$

For the approximation of the above problem, we use the Forward Euler scheme:

$$\Phi_{p,q}^{m+1} = \Phi_{p,q}^m + \tau \left(\mathcal{J}^m[F^m] \right),$$

where F^m is the approximation of the reduced distribution function (1) at time t^m .

For stability, the subtime step τ is chosen to satisfy the Courant-Friedrichs-Lewy (CFL) condition (see, e.g., [30]):

$$\max \left\{ \frac{\tau}{\Delta x}, \frac{\tau}{\Delta y} \right\} \leq 1.$$

4 Numerical results

We present a series of numerical results to showcase the features of our model. We start from the simulation of evacuation from a room with one exit in Section 4.1. We use this first test to validate our implementation of the model presented in Section 2 against the results in [1]. In order to further validate our software, in Section 4.2 we compare our numerical results with the experimental data reported in [40], where the authors study the evacuation from a room with two exits. Our successfully validated code is then used to study evacuation from a room with obstacles in Section 4.3 and lane formation in a corridor in Section 4.4.

For all the simulations, we consider eight different velocity directions $N_d = 8$ in the discrete set:

$$I_\theta = \left\{ \theta_i = \frac{i-1}{8} 2\pi : i = 1, \dots, 8 \right\}.$$

4.1 Evacuation from a room with one exit

This first test case is taken from [1]. The computational domain encloses a square room with side 10 m with an exit door located in the middle of the right side. The exit size is 2.6 m. The computational domain is larger than the room itself to follow the motion of the pedestrian also once they have left the room. We aim at simulating the evacuation of 46 people located inside the room and initially distributed into two equal-area circular clusters. See Figure 3, top left panel. The two groups are initially moving against the each other with opposite initial directions θ_3 and θ_7 . Following [1], simulations are performed with $\varepsilon = 0.4$.

In order to work with dimensionless quantities as described in Section 2, we define the following reference quantities: $D = 10\sqrt{2}$ m, $V_M = 2$ m/s, $T = D/V_M = 5\sqrt{2}$ s, and $\rho_M = 7$ people/m². However, once the results are computed we convert them back to dimensional quantities.

In order to understand what level of refinement is needed for the mesh, we consider three different meshes:

- *coarse mesh* with $\Delta x = \Delta y = 0.5$ m;
- *medium mesh* with $\Delta x = \Delta y = 0.25$ m;
- *fine mesh* with $\Delta x = \Delta y = 0.125$ m.

Similarly, we consider three different time steps: a large time step $\Delta t_{large} = 1.5$ s, a medium time step $\Delta t_{medium} = 0.75$ s, and a small time step $\Delta t_{small} = 0.375$ s. The value of M for the Lie

splitting scheme is set to 3. Figure 3 shows the density computed with medium mesh and Δt_{medium} at times $t = 0, 1.5, 3, 6, 10.5, 13.5$ s.

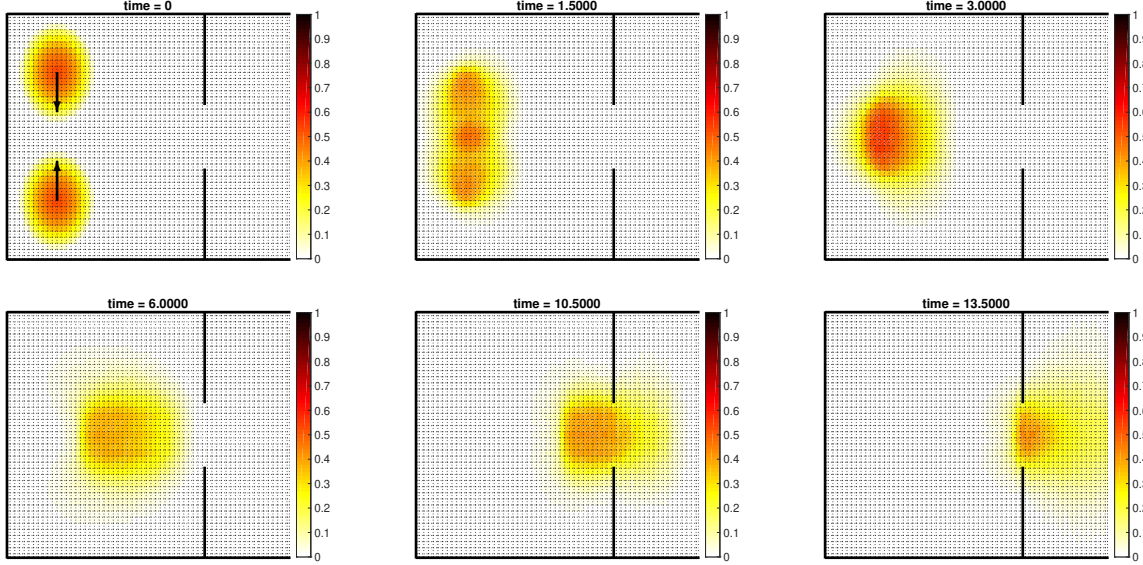


Figure 3: Evacuation process of 46 pedestrians grouped into two clusters with opposite initial directions θ_3 and θ_7 using the medium mesh and Δt_{medium} for time $t = 0, 1.5, 3, 6, 10.5, 13.5$ s. The color refers to density.

Figure 4 (A) reports the number of pedestrians left in the room computed with the following combinations of mesh and time step: coarse mesh and Δ_{large} , coarse mesh and Δ_{medium} , coarse mesh and Δ_{small} , medium mesh and Δ_{medium} , medium mesh and Δ_{small} , and fine mesh and Δ_{small} . In all the cases the total evacuation time is around 18 s, which agrees well with the results reported in [1]. However, we see that the evacuation dynamics varies when the mesh and time step change. In fact, from Figure 4 (A) one can observe that as the time step gets smaller with a given mesh people walk slightly faster, while as the mesh gets finer with a given time step pedestrians walk slightly slower. When using operator splitting methods, it is advised to reduce the time step as the mesh is refined (see, e.g. [23]). So, for ease of comparison in Figure 4 (B) we report only the results computed with coarse mesh and Δ_{large} , medium mesh and Δ_{medium} , fine mesh and Δ_{small} . We can see very good agreement for those three curves.

Next, we consider the same room as in the previous test but we vary the exit size. We locate the exit symmetrically with respect to the room centerline and let the exit size vary from 1.5 m to 4 m. We consider the medium meshes and Δt_{medium} mentioned before since Figure 4 show that is an appropriate choice for the problem under consideration. All the other model and discretization parameters are set like in the previous test. Figure 5 shows the total evacuation time as a function

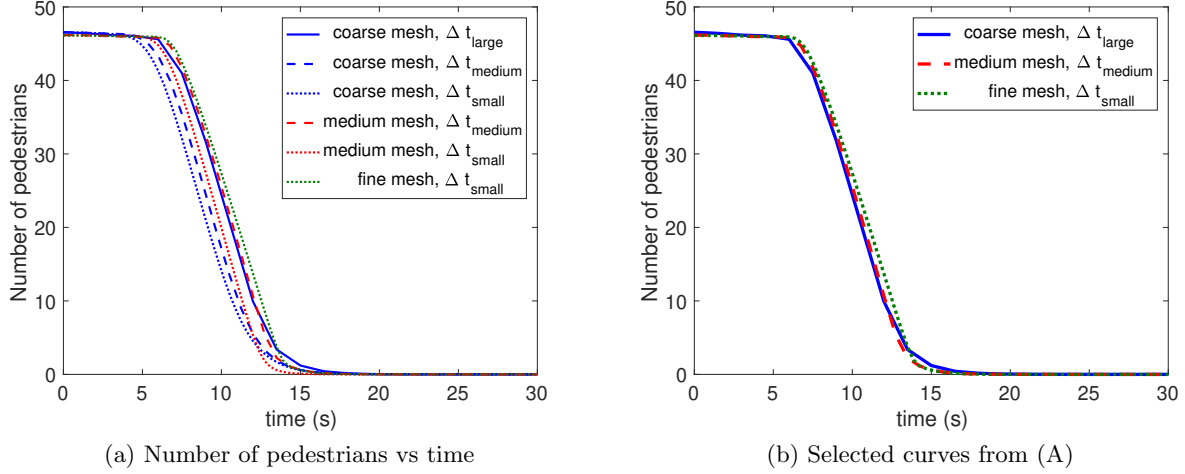


Figure 4: (A) Number of pedestrians inside the room over time computed with six different combinations of mesh and time step. For ease of comparison, (B) shows only the curves in (A) obtained with simultaneous refinements of mesh and time step.

of the exit size. First, we notice that our results are in very good agreement with the results reported in [1]. As expected, the total evacuation time decreases with the exit size, but that once the exit is large enough for the crowd contained in the room the evacuation time does not change significantly if the exit is further enlarged.

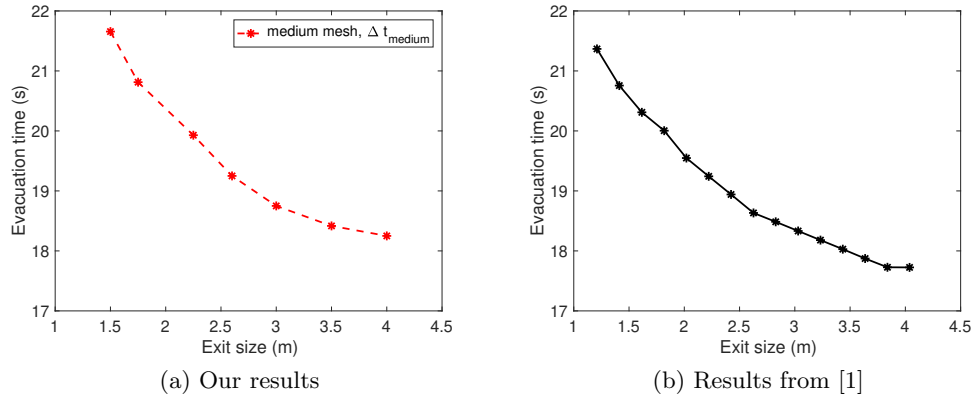


Figure 5: Computed evacuation time from the room with one exit versus the exit size: (A) our results and (B) results from [1].

As last test for the room with one exit, we computed the total evacuation time from a room with variable exit size for different values of ε . The results did not show any visible difference from the ones displayed in Figure 5 (A), which corresponds to $\varepsilon = 0.4$, and thus are not reported here. This test case is probably too simple to see any difference in the crowd dynamics when (F3), i.e. the tendency avoid the crowd, is dominant over (F4), i.e. the tendency to follow the crowd, and viceversa.

4.2 Evacuation from a room with two exits

After validating our software against the numerical results in [1], we proceed with the validation against the experimental data reported in [40]. The computational domain corresponds to the setting studied in [40]: a room of side 10 m with different sized exits placed on the right side: exit 1 with size 0.7 m and exit 2 with size 1.1 m. The distance between the two exits is 3 m. See Figure 6.

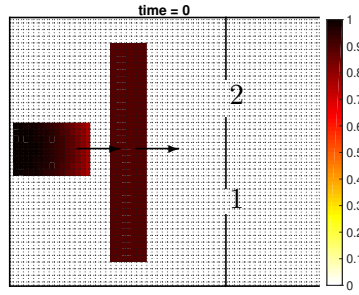


Figure 6: Computational domain corresponding to the experimental set-up in [40] and initial density and direction (i.e., θ_1) for the experiment with 138 pedestrians.

The data in [40] refer to ten trials: 2 trials with 18 pedestrians, 6 trials with 40 pedestrians, and 2 trials with 138 pedestrians. In the experiments with 18 and 40 pedestrians (and so in the simulation as well), the group is initially positioned in a square located symmetrically with respect to the horizontal axis of the room and towards the back of the room with linearly increasing people density from the front to the back. In the experiments with 138 pedestrians, pedestrians are initially distributed as follows: a first group of 90 people is positioned in a rectangle in the middle of the room, while the remaining 48 people are positioned in a square behind the first group. Thus, we adopt the same configuration in the simulations. We impose constant density in the rectangle and prescribe a linearly increasing density from the front to the back of the square. See Figure 6. In all the cases, the pedestrians are given initial direction θ_1 . For all the simulations, we use the medium mesh and Δt_{small} considered in Section 4.1.

To compute the mean density D_V and mean flow rate F_V we use the Voronoi method [38]:

$$D_V(t) = \frac{\sum_{\mathbf{x} \in \omega} \rho(t, \mathbf{x})}{|\omega|}, \quad F_V(t) = D_V V_V E, \quad (15)$$

where V_V is the mean velocity modulus over the area ω and E is the exit width. We choose two 4 m^2 areas in front of the exits as ω . The mean density and mean flow rate computed from our simulations are shown in Figure 7 (A) and (B). Figure 7 (C) and (D) report the measured mean density and mean flow rate from the experiments in [40]. We see very good agreement between computed and measured quantities for the 40 and 138 people cases, while there is no good agreement for the 18 people case. This is to be expected since the kinetic approach is not meant to simulate the dynamics of a small number of pedestrians. With this test we conclude the validation of our software.

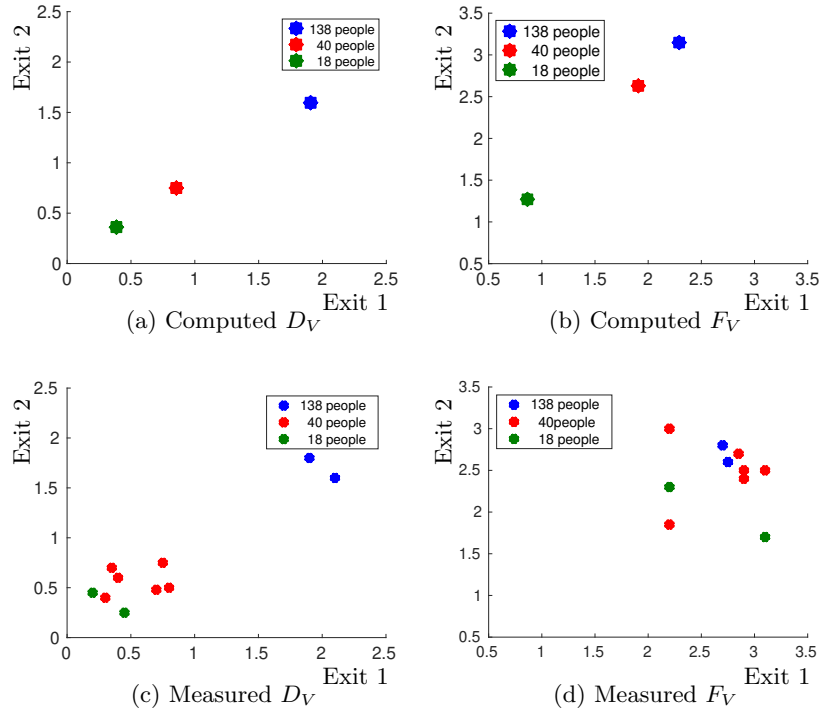


Figure 7: Computed (A) mean density D_V and (B) mean flow rate F_V as defined in (15), and measured (C) mean density and (D) mean flow rate from [40].

So far, we have only considered velocity modulus v as defined (3), which uses a cubic polynomial

outside the free flow regime. For the two exit test, we take into consideration other possible choices:

$$\begin{aligned} v_{purple}(\rho) &= (1 + \cos((\rho - 0.2)^{\frac{2}{3}}\pi/0.8^{\frac{2}{3}}))/2, \\ v_{orange}(\rho) &= (1 + \cos((\rho - 0.2)^{\frac{1}{2}}\pi/0.8^{\frac{1}{2}}))/2, \\ v_{blue}(\rho) &= (1 + \cos((\rho - 0.2)^{\frac{1}{3}}\pi/0.8^{\frac{1}{3}}))/2. \end{aligned} \quad (16)$$

See Figure 8 (A). We repeat the test with 138 pedestrians for all the above velocity moduli. The corresponding number of pedestrians in the room versus times is shown in Figure 8 (B). For a given density $\bar{\rho}$ in the slowdown zone, we have $v(\bar{\rho}) > v_{purple}(\bar{\rho}) > v_{orange}(\bar{\rho}) > v_{blue}(\bar{\rho})$. Thus, it is not surprising the the total evacuation time increases as we pass from the original definition of velocity modulus in (3) to v_{blue} through v_{purple} and v_{orange} . To further illustrate the difference in the evacuation process when the above velocity moduli are used, in Figure 9 we display the density and velocity modulus (with selected velocity vectors) at time $t = 15$ when using the three velocity moduli.

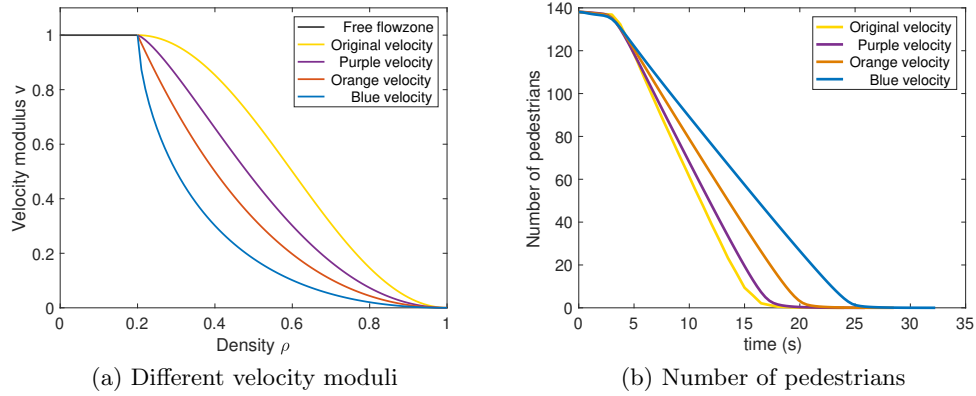


Figure 8: (A) Different velocity moduli under consideration and (B) corresponding number of pedestrians in the room versus time for the 138 pedestrian case.

Next, we investigate the relationship between evacuation time and the width ratio of the two exits. We fix the size and position of exit 1, and the position of the center of exit 2, while the size of exit 2 varies. See Figure 10 (A) for the widths of exit 2 under consideration and corresponding width ratios. We consider two scenarios: the group of 40 people with velocity modulus (3) and the group of 138 people with the blue velocity modulus (16). In both cases, all other model and discretization parameters are set like for the results reported in Figure 7. Figure 10 (B) shows the total evacuation time versus the exit width ratio for both scenarios. As expected, when the ratio of exit 2 width/exit 1 width increases the total evacuation time decreases.

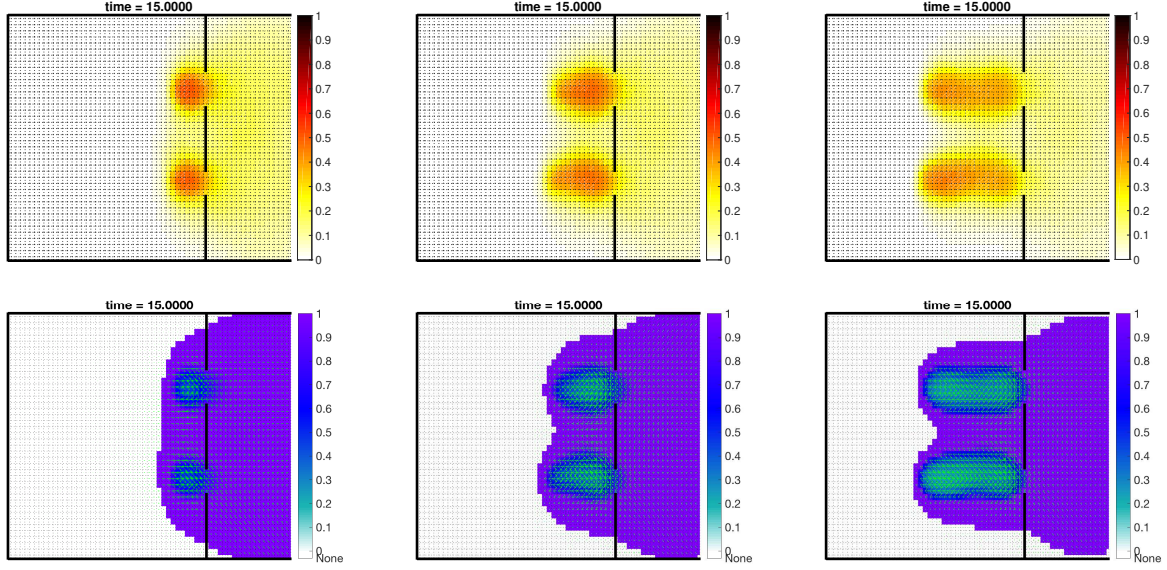


Figure 9: Density (top) and velocity magnitude with selected velocity vectors (bottom) for the evacuation process of 138 pedestrians with the purple (left), orange (middle), and blue (right) velocity moduli at time $t = 15$ s.

4.3 Evacuation from a room with obstacles

In the model introduced in Section 2.1, parameter α represents the quality of the environment, which influences also the maximal dimensionless velocity modulus (3) a pedestrian can reach. In theory, parameter $\alpha = 0$ forces pedestrians to stop, while the value $\alpha = 1$ contributes to keep the maximal velocity modulus. However, in practice this parameter alone is not sufficient to model obstacles within the domain. To effectively model the obstacles, we use the strategy reported in Section 2.1.2.

We consider a square room of side 10 m with a 2.6 m wide exit located on the right wall as in Section 4.1, with the following obstacle configuration:

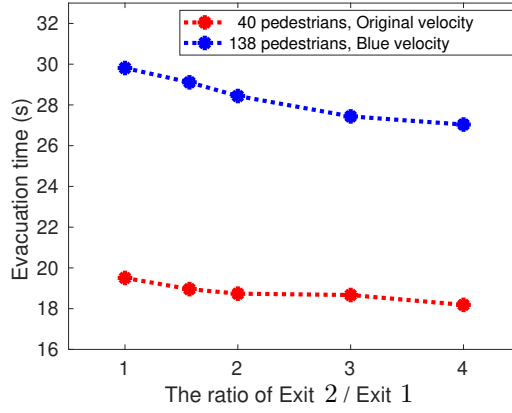
1. One obstacle close to the exit, i.e. in the middle of the right wall, with effective area depicted in Figure 11 (A).
2. Two obstacles close to the right wall, placed symmetrically with respect to the exit. See Figure 11 (B) for the effective area of both obstacles.

Pedestrians are initially distributed in a rectangular region with constant density $\rho = 0.80$, as shown in Figure 11. The total number of pedestrians is 44. The initial direction is θ_1 .

Figure 12 and 13 show the evacuation process for configuration 1 when $\alpha = 1$ and $\alpha = 0$ in the effective area, respectively. As explained in Section 2.1.2, when $\alpha = 1$ (resp., $\alpha = 0$) pedestrians

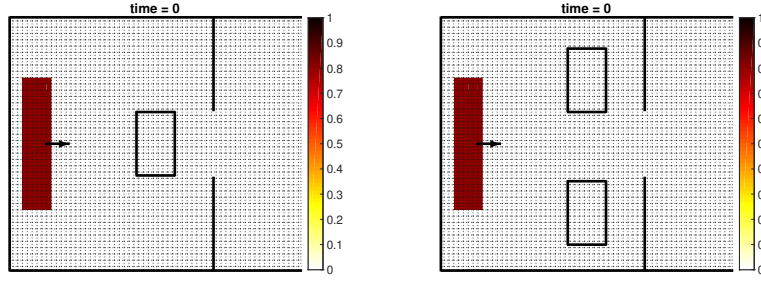
Exit 2 (m)	Ratio of Exit 2 / Exit 1
0.7	1
1.1	1.5714
1.4	2
2.1	3
2.8	4

(a) Exit 2 width and width ratios



(b) Evacuation time vs width ratio

Figure 10: (A) Widths of exit 2 under consideration and corresponding width ratios and (B) evacuation time versus width ratios for two different scenarios.



(a) Configuration 1

(b) Configuration 2

Figure 11: Computational domain with effective area for (A) an obstacle placed in the middle of the room, towards the exit, and (B) two obstacles placed symmetrically with respect to the exit.

avoid the front (resp., back) part of the effective area. Moreover, the shape of the real obstacle is different: it is square for $\alpha = 1$, while for $\alpha = 0$ it is slender. These findings are confirmed by Figure 14 and 15, which show the evacuation process for configuration 2 when $\alpha = 1$ and $\alpha = 0$ in the effective area, respectively.

Finally, Figure 16 compares the evacuation times for the room with no obstacles ($\alpha = 1$ everywhere in the domain), and for configurations 1 and 2 for $\alpha = 1$ and $\alpha = 0$ in the effective area.

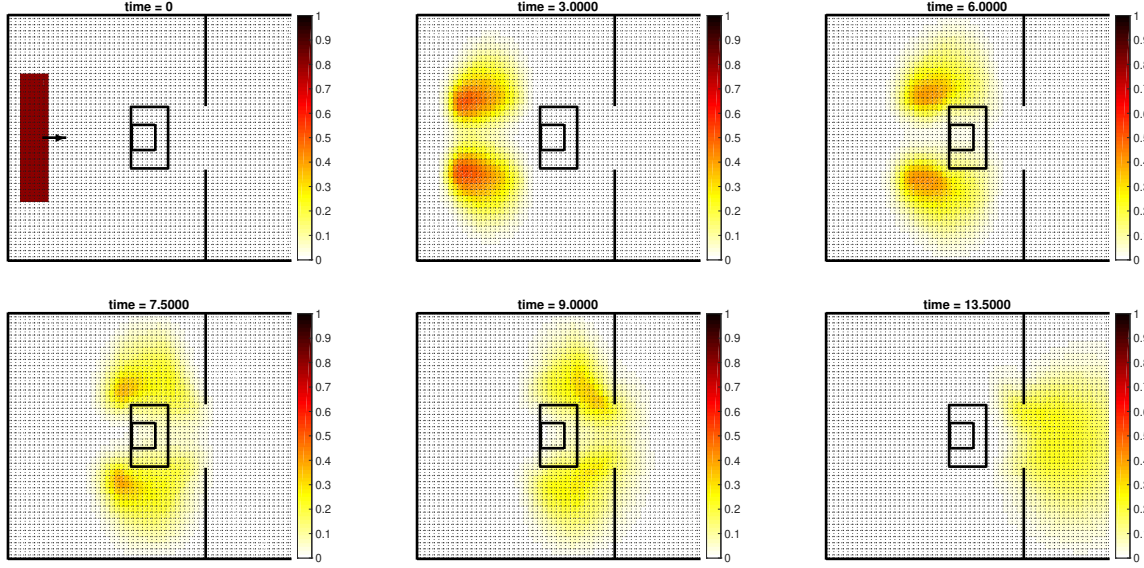


Figure 12: Configuration 1 with $\alpha = 1$ in the effective area: computed density for $t = 0, 3, 6, 7.5, 9, 13.5$ s. The small square within the effective area represents the real obstacle.

Obviously, the shortest evacuation time is for the room with no obstacles and overall good quality of the environment. The evacuation time is slightly larger when there is one or two obstacles and α is equal to 1 in the effective area. When we compare Figure 12 and 13 at $t = 13.5$ s, it seems that roughly the same number of people is left in the room. However, the small group of people in the effective area in Figure 13 has velocity modulus close 0 since α is equal to 0 there and thus the overall evacuation process takes longer. The same happens in Figure 15.

4.4 Lane formation

In this section, we assess the ability of our model to reproduce an empirically observed phenomenon: formation of lanes in a corridor when two or more groups of pedestrians have opposite walking directions [25]. We consider a computational domain of length $L = 20$ m and width $H = 5$ m and we impose periodic boundary conditions on the short edges. The reference quantities we use for this test are: $D = 5\sqrt{17}$ m, $V_M = 2$ m/s, and $\rho_M = 7$ per/m². See Section 2. The reference time is thus $T_M = 5\sqrt{17}/2$ s.

We generate a mesh with $\Delta x = \Delta y = 0.2$ m and set $\Delta t = 0.3$ s. We run two tests: in one 98 people are present in the computational domain, while in the other we increase the number of people to 188. Pedestrians are initially distributed into four equal-area rectangular clusters with a parabolic density distribution with maximum density $\rho = 1$ in the center and minimum

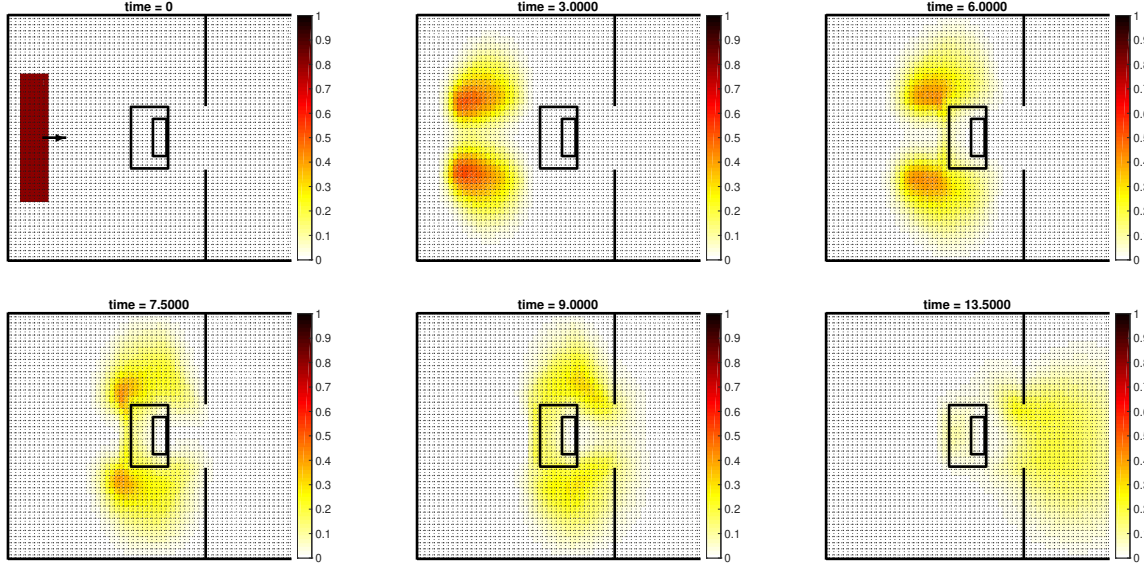


Figure 13: Configuration 1 with $\alpha = 0$ in the effective area: computed density for $t = 0, 3, 6, 7.5, 9, 13.5$ s. The small rectangle within the effective area represents the real obstacle.

density $\rho = 0.6$. The groups at the opposite ends of the corridor initially move with opposite initial directions θ_1 and θ_5 . See the top left panel in Figure 17 and 18. The rest of Figure 17 and 18 shows the evolution of the pedestrian dynamics. From both pictures, we see that pedestrians try to avoid contact by changing the direction, which leads to sorting, separation, and lane formation.

5 Conclusion

We considered a kinetic theory approach to model pedestrian dynamics in bounded domain and adapted it to handle obstacles. For the numerical approximation of the solution to our model, we applied the Lie splitting scheme which breaks the problem into two pure advection problems and a problem involving the interaction with the environment and other pedestrians.

Several test cases have been considered in order to show the ability of the model to reproduce qualitatively:

- evacuation from a room with one exit, without and with obstacles;
- evacuation from a room with two exits and no obstacles;
- lane formation.

In the case of the room with two exits and no obstacles, we also presented a quantitative comparison with experimental data. Numerical results and experimental data are in very good agreement for medium and medium-to-large groups of people. With the confidence in the model given by the

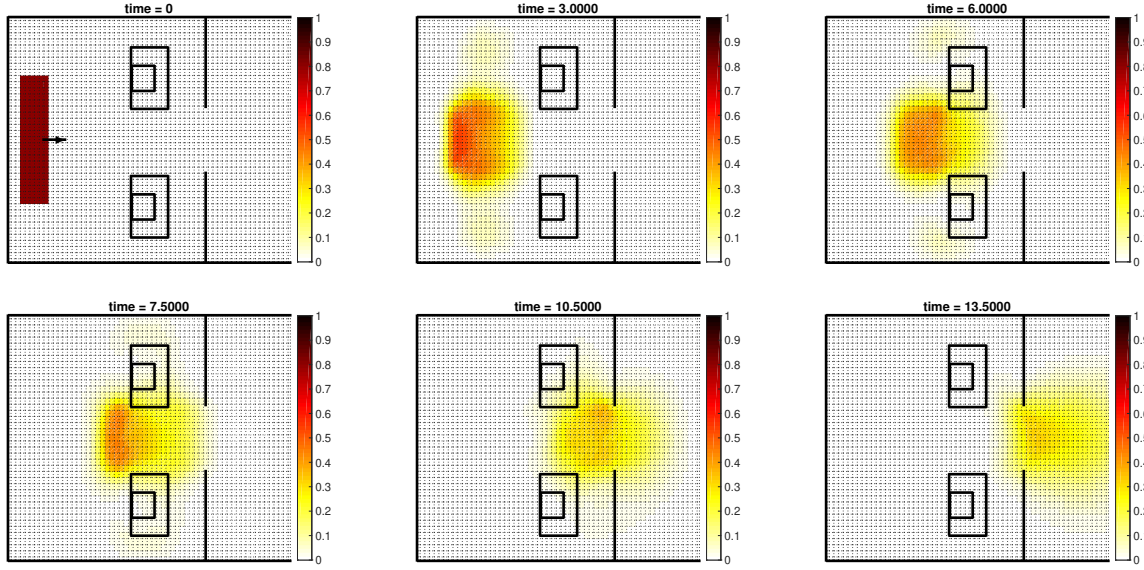


Figure 14: Configuration 2 with $\alpha = 1$ in the effective area: computed density for $t = 0, 3, 6, 7.5, 10.5, 13.5$ s. The small square within the effective area represents the real obstacle.

experimental validation, we performed numerical tests to study evacuation for different scenarios in terms of exit sizes, obstacle shapes, and velocity moduli.

Acknowledgements

This work has been partially supported by NSF through grant DMS-1620384.

References

- [1] J. P. Agnelli, F. Colasuonno and D. Knopoff, A kinetic theory approach to the dynamics of crowd evacuation from bounded domains, *Mathematical Models and Methods in Applied Sciences*, **25** (2015), 109–129.
- [2] G. Antonini, M. Bierlaire and M. Weber, Discrete choice models of pedestrian walking behavior, *Transportation Research Part B: Methodological*, **40** (2006), 667–687.
- [3] M. Asano, T. Iryo and M. Kuwahara, Microscopic pedestrian simulation model combined with a tactical model for route choice behaviour, *Transportation Research Part C: Emerging Technologies*, **18** (2010), 842–855.

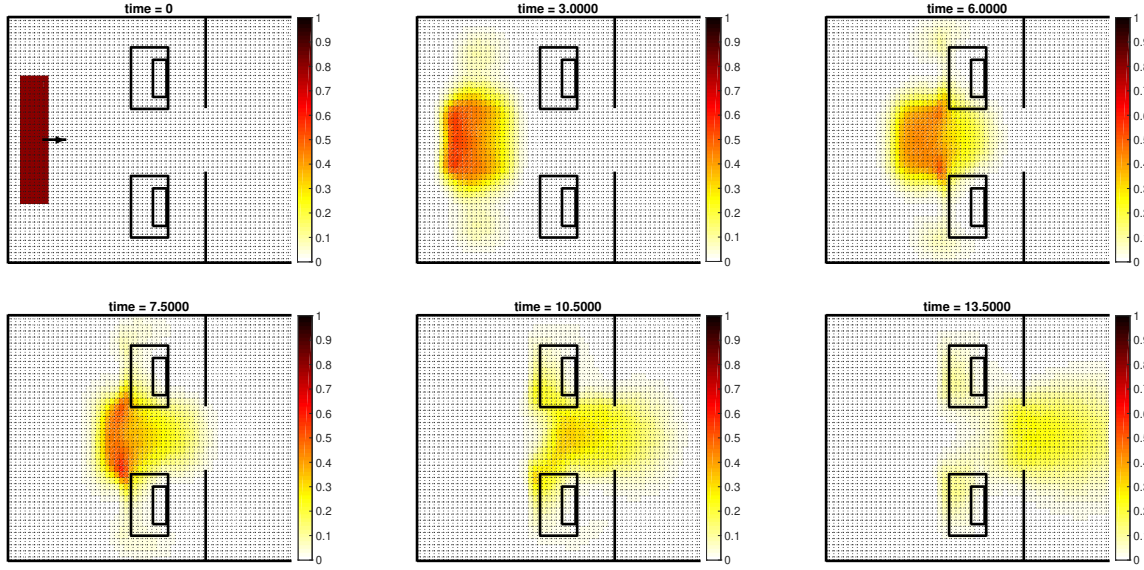


Figure 15: Configuration 2 with $\alpha = 0$ in the effective area: computed density for $t = 0, 3, 6, 7.5, 10.5, 13.5$ s. The small rectangle within the effective area represents the real obstacle.

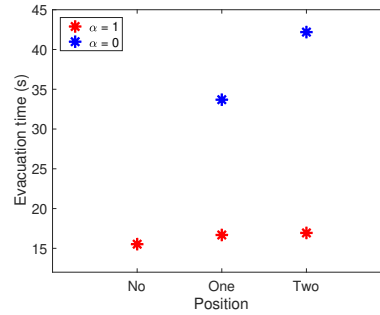


Figure 16: Evacuation times for the room with no obstacles ($\alpha = 1$ everywhere in the domain), for room with one and two obstacles with $\alpha = 1$ and $\alpha = 0$ in the effective area.

- [4] S. Bandini, S. Manzoni and G. Vizzari, Agent based modeling and simulation: An informatics perspective, *Journal of Artificial Societies and Social Simulation*, **12** (2009).
- [5] N. Bellomo and A. Bellouquid, On the modeling of crowd dynamics: Looking at the beautiful shapes of swarms, *Networks and Heterogeneous Media*, **6** (2011), 383–399.
- [6] N. Bellomo, A. Bellouquid and D. Knopoff, From the microscale to collective crowd dynamics,

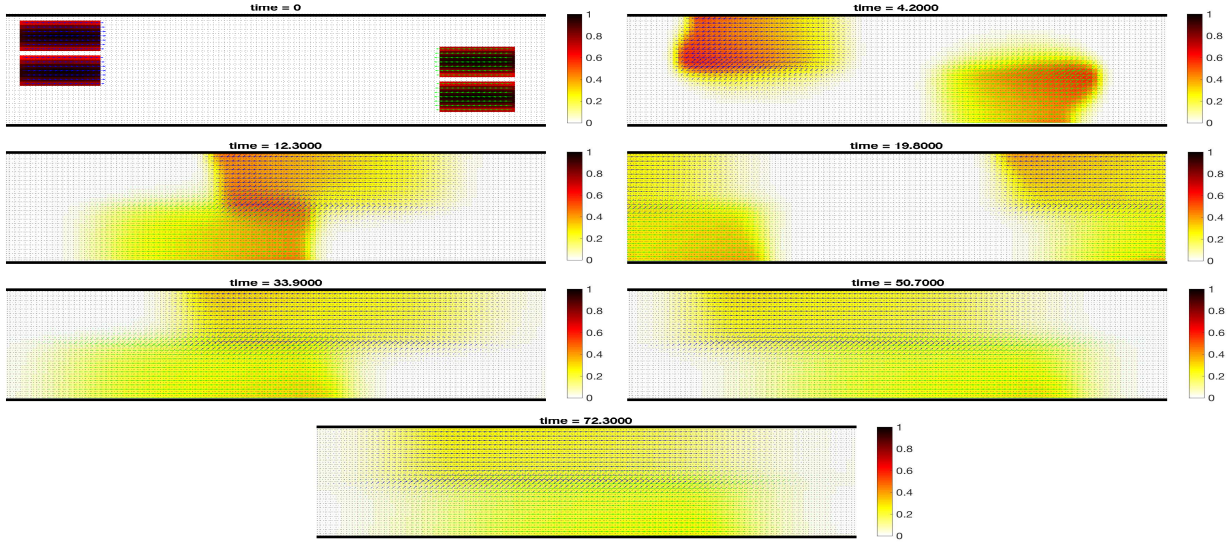


Figure 17: The movement process of 98 pedestrians grouped into four clusters with opposite initial direction θ_1 and θ_5 in the periodic corridor for $t = 0, 4.2, 12.3, 19.8, 33.9, 50.7, 72.3$ s, respectively.

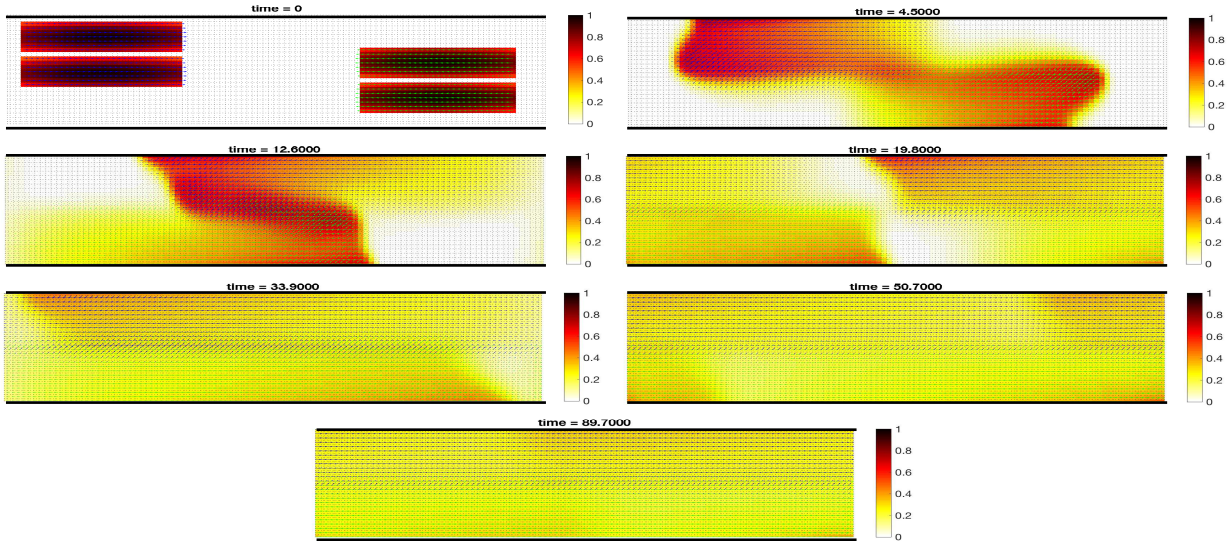


Figure 18: The movement process of 188 pedestrians grouped into four clusters with initial opposite direction θ_1 and θ_5 in the periodic corridor for $t = 0, 4.5, 12.6, 19.8, 33.9, 50.7, 89.7$ s, respectively.

943–963.

- [7] N. Bellomo, A. Bellouquid, L. Gibelli and N. Outada, *A Quest Towards a Mathematical Theory of Living Systems*, Modeling and Simulation in Science, Engineering and Technology, Birkhauser, 2017.
- [8] N. Bellomo and C. Dogbe, On the modeling of traffic and crowds: A survey of models, speculations, and perspectives, *Society for Industrial and Applied Mathematics Review*, **53** (2011), 409–463.
- [9] N. Bellomo and L. Gibelli, Toward a mathematical theory of behavioral-social dynamics for pedestrian crowds, *Mathematical Models and Methods in Applied Sciences*, **25** (2015), 2417–2437.
- [10] N. Bellomo and L. Gibelli, Behavioral crowds: Modeling and Monte Carlo simulations toward validation, *Computers and Fluids*, **141** (2016), 13–21.
- [11] N. Bellomo, L. Gibelli and N. Outada, On the interplay between behavioral dynamics and social interactions in human crowds, *Kinetic and Related Models*, **12** (2019), 397–409.
- [12] N. Bellomo, D. Knopoff and J. Soler, On the difficult interplay between life, “Complexity”, and mathematical sciences, *Mathematical Models and Methods in Applied Sciences*, **23** (2013), 1861–1913.
- [13] N. Bellomo, B. Piccoli and A. Tosin, Modeling crowd dynamics from a complex system viewpoint, *Mathematical Models and Methods in Applied Sciences*, **22** (2012).
- [14] V. J. Blue and J. L. Adler, Cellular automata microsimulation of bidirectional pedestrian flows, *Journal of Transportation Research Record*, **1678** (1999), 135–141.
- [15] V. J. Blue and J. L. Adler, Cellular automata microsimulation for modeling bi-directional pedestrian walkways, *Transportation Research Part B: Methodological*, **35** (2000), 293–312.
- [16] C. Burstedde, K. Klauck, A. Schadschneider, J. Zittartz, Simulation of pedestrian dynamics using a two-dimensional cellular automaton, *Physica A: Statistical Mechanics and its Applications*, **295** (2001), 507–525.
- [17] N. Chooramun, P. J. Lawrence and E. R. Galea, An agent based evacuation model utilising hybrid space discretisation, *Safety Science*, **50** (2012), 1685–1694.
- [18] M. Chraïbi, U. Kemloh, A. Schadschneider and A. Seyfried, Force-based models of pedestrian dynamics, *Networks and Heterogeneous Media*, **6** (2011), 1556–1801.

- [19] M. Chraïbi, A. Tordeux, A. Schadschneider and A. Seyfried, *Modelling of Pedestrian and Evacuation Dynamics*, Encyclopedia of Complexity and Systems Science Series, 2019, 649–669.
- [20] J. Dai, X. Li and L. Liu, Simulation of pedestrian counter flow through bottlenecks by using an agent-based model, *Physica A: Statistical Mechanics and its Applications*, **392** (2013), 2202–2211.
- [21] J. Dijkstra, J. Jessurun and H. Timmermans, A multi-agent cellular automata model of pedestrian movement, *Pedestrian and Evacuation Dynamics*, (2001), 173–181.
- [22] B. Einarsson, *Accuracy and Reliability in Scientific Computing*, Society for Industrial and Applied Mathematics, 2005.
- [23] R. Glowinski, *Finite Element Methods for Incompressible Viscous Flow*, Handbook of numerical analysis, **9**. North-Holland, Amsterdam, 2003.
- [24] D. Helbing, A mathematical model for the behavior of pedestrians, *Behavioral Science*, **36** (1991), 298–310.
- [25] D. Helbing, I. J. Farkas, P. Molnar, and T. Vicsek, Simulation of pedestrian crowds in normal and evacuation situations, *Pedestrian and Evacuation Dynamics*, **21** (2002), 21–58.
- [26] D. Helbing and P. Molnar, Social force model for pedestrian dynamics, *Physical Review E*, **51** (1998), 4282–4286.
- [27] D. Helbing and T. Vicsek, Optimal self-organization, *New Journal of Physics*, **1** (1999).
- [28] R. L. Hughes, A continuum theory for the flow of pedestrians, *Transportation Research Part B: Methodological*, **36** (2002), 507–535.
- [29] A. Johansson, D. Helbing and P. K. Shukla, Specification of the social force pedestrian model by evolutionary adjustment to video tracking data, *Advances in Complex Systems*, **10** (2007), 271–288.
- [30] R. J. LeVeque, *Numerical Methods for Conservation Laws*, 2nd edition, Springer Science & Business Media, 1992.
- [31] X. Li, X. Yan, X. Li and J. Wang, Using cellular automata to investigate pedestrian conflicts with vehicles in crosswalk at signalized intersection, *Discrete Dynamics in Nature and Society*, (2012).
- [32] S. Liu, S. Lo, J. Ma and W. Wang, An agent-based microscopic pedestrian flow simulation model for pedestrian traffic problems, *IEEE Transactions on Intelligent Transportation Systems*, **15** (2014), 992–1001.

- [33] J. Moussaïd, D. Helbing, S. Garnier, A. Johansson, M. Combe and G. Theraulaz, Experimental study of the behavioural mechanisms underlying self-organization in human crowds, *Proceedings of the Royal Society B: Biological Sciences*, **276** (2009), 2755–2762.
- [34] A. Schadschneider, W. Klingsch, H. Kluepfel, T. Kretz, C. Rogsch, A. Seyfried, Evacuation dynamics: Empirical results, modeling and applications, *Extreme Environmental Events: Complexity in Forecasting and Early Warning*, (2011), 517–550.
- [35] A. Schadschneider and A. Seyfried, Empirical results for pedestrian dynamics and their implications for modeling, *Networks and Heterogeneous Media*, **6** (2011), 545–560.
- [36] A. Seyfried, O. Passon, B. Steffen, M. Boltes, T. Rupperecht and W. Klingsch, New insights into pedestrian flow through bottlenecks, *Transportation Science*, **43** (2009), 395–406.
- [37] A. Shende, M. P. Singh and P. Kachroo, Optimization-Based feedback control for pedestrian evacuation from an exit corridor, *IEEE Transactions on Intelligent Transportation Systems*, **12** (2011), 1167–1176.
- [38] B. Steffen and A. Seyfried, Methods for measuring pedestrian density, flow, speed and direction with minimal scatter, *Physica A: Statistical Mechanics and its Applications*, **389** (2009), 1902–1910.
- [39] A. Turner and A. Penn, Encoding Natural Movement as an Agent-Based System: An Investigation into Human Pedestrian Behaviour in the Built Environment, *Environment and Planning B: Planning and Design*, **29** (2002), 473–490.
- [40] A. U. K. Wagoum, A. Tordeux and W. Liao, Understanding human queuing behaviour at exits: an empirical study, *Royal Society Open Science*, **4** (2017).
- [41] J. A. Ward, A. J. Evans and N. S. Malleson, Dynamic calibration of agent-based models using data assimilation, *Royal Society Open Science*, **3** (2016).
- [42] J. Zhang, W. Klingsch, A. Schadschneider and A. Seyfried, Transitions in pedestrian fundamental diagrams of straight corridors and T-junctions, *Journal of Statistical Mechanics: Theory and Experiment*, **6** (2011).
- [43] B. Zhou, X. Wang and X. Tang, Understanding collective crowd behaviors: Learning a Mixture model of Dynamic pedestrian-Agents, *2012 IEEE Conference on Computer Vision and Pattern Recognition*, (2012), 2871–2878.